Available online at www.sciencedirect.com

ScienceDirect

Procedia IUTAM 16 (2015) 60 – 69

Procedia IUTAM

www.elsevier.com/locate/procedia

IUTAM Symposium on Dynamics of Capsules, Vesicles and Cells in Flow

Electric field induced deformations of biomimetic fluid membranes

Paul F. Salipante[a], Mark L. Shapiro[a], Petia M. Vlahovska[a,*]

[a] *School of Engineering, Brown University, Providence RI 02912, USA*

Abstract

We investigate the coupling between the mechanics of fluid membranes and transmembrane electric potential using as a model system the giant vesicle (closed bilayer membrane made of lipids or polymers). In DC electric pulses, an initially quasispherical giant vesicle can become a spherocylinder. The edge between the spherical cap and the cylindrical section appears to separate porated (conducting) and intact (insulating) regions of the membrane. The location of the edge provides a quick estimate for the critical poration voltage of a membrane. A uniform AC electric field affects membrane fluctuations, increasing the effective bending rigidity and decreasing the effective membrane tension. Moreover, a very deflated vesicle can become an asymmetric dumbbell. In the case of multicomponent membranes, the miscibility temperature (at which domains form in an initially homogeneous membrane) decreases with applied electric field strength.

Peer-review under the responsibility of the organizing committee of DYNACAPS 2014 (Dynamics of Capsules, Vesicles and Cells in Flow).

Keywords: Electroporation, Electrohydrodynamics, Giant vesicle, Leaky dielectric

1. Introduction

The interaction of biological membranes with exogenous and endogenous electric fields underlies many physiological and technological processes, from morphogenesis to electroporation. The plasma membrane plays a central role in establishing the electric properties (resting, active, and passive) of the cell, through its regulation of the transport of ions between the extracellular and intracellular spaces. Yet, very little is known about the physical mechanisms underlying the interaction of biological membranes and electric fields, in particular, the biomembrane deformation induced by electric stresses.

1.1. Physical picture

Let us consider a vesicle made of an ion-impermeable charge-free bilayer membrane with dielectric constant, $\epsilon_{\rm mm}$, viscosity, $\mu_{\rm mm}$, and thickness, d. The fluids inside and outside the vesicle are aqueous solutions with different con-

* Corresponding author. Tel.: +1-401-863-9774 ; fax: +1-401-863-9028.
E-mail address: petia_vlahovska@brown.edu

Peer-review under the responsibility of the organizing committee of DYNACAPS 2014 (Dynamics of Capsules, Vesicles and Cells in Flow).
doi:10.1016/j.piutam.2015.03.008

ductivities, λ_{in} and λ_{ex}, e.g., due to different salt concentrations. This mismatch in the bulk fluid electrical properties is characterized by the conductivity ratio

$$R = \frac{\lambda_{\text{in}}}{\lambda_{\text{ex}}}. \tag{1}$$

The solutions' viscosities and dielectric constants are nearly the same (basically equal to those of water).

Application of an electric field leads to accumulation of ions at the membrane surfaces and the vesicle acts as a capacitor. For a quasi–spherical vesicle made of an insulating (ion-impermeable) membrane the characteristic time scale for the charging process is [1,2,3],

$$t_{\text{mm}} = \frac{aC_{\text{mm}}}{\lambda_{\text{in}}}\left(1 + \frac{R}{2}\right), \tag{2}$$

where $C_{\text{mm}} = \epsilon_{\text{mm}}/d$ is the capacitance of the membrane and a is the vesicle radius. For systems with typical solution conductivity $\lambda \sim 0.1\mu$S/cm and $a \sim 10\mu$m the charging timescale is $t_{\text{mm}} \sim 1$ms.

Membrane capacitance sets up a transmembrane potential, which in an uniform DC electric field, $\mathbf{E}^{\infty} = E_0\hat{\mathbf{z}}$, evolves toward steady state as [4]

$$V_{\text{mm}} = \frac{3}{2}aE_0\left(1 - \exp\left(-t/t_{\text{mm}}\right)\right)\cos(\theta), \tag{3}$$

where θ is the angle between the electric field direction and position at the interface.

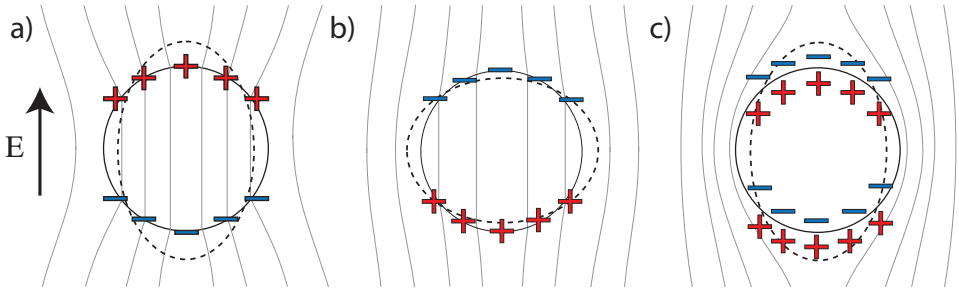

Fig. 1. Sketch of the electric field and induced charge distribution around a vesicle immersed in an electrolyte solution, following the imposition of a uniform DC field (a) $t < t_{\text{mm}}$ and $R > 1$ (b) $t < t_{\text{mm}}$ and $R < 1$ (c) fully charged membrane capacitor $t \gg t_{\text{mm}}$, any R. The dashed lines indicate the vesicle deformation.

During the charging process, $t < t_{\text{mm}}$ (or in AC fields $\omega^{-1} < t_{\text{mm}}$), the ion densities on the inner and outer membrane surfaces may become temporarily unbalanced. This is due to the difference in the conduction rates in the inner and suspending solutions, which is characterized by R. The polarity of the apparent charge (and resulting vesicle deformation) is illustrated in Figure 1. At steady state however, $t \gg t_{\text{mm}}$, irrespective of R the capacitor is fully charged, the apparent charge is zero, and the electric field is expelled from the vesicle interior.

Upon application of a DC field, a vesicle with $R < 1$ will initially deform into an oblate spheroid but eventually adopts a prolate shape [4]. This theoretical prediction has been confirmed experimentally and with numerical simulations [5]. Our previous work explored the limits where the membrane remains insulating. Poration makes the membrane conducting, which suppresses the prolate deformation for $R < 1$ [5], destabilizes the membrane [6] and likely causes the drum–like shapes [7] which we analyze here.

1.2. Methods

Giant vesicles from lipids and diblock copolymers (PBd-b-PEO) are made using the electroformation method in a 100 mM sucrose solution without the addition of salt. The vesicles are diluted into osmotically matched 100 mM glucose solution to ensure constant volume throughout the experiment. A small amounts of sodium chloride (less than 1 mM) is added to the exterior glucose solution to adjust conductivty. Vesicles are observed using a phase contrast

microscopy and recorded using a high speed camera (Photron SA1.1). Vesicles are observed in an Eppendorf Micro-Fusion chamber (Eppendorf, Germany), consisting of a teflon frame supporting a pair of cylindrical electrodes 0.5 mm apart fixed to a lower cover glass. The temperature of the chamber was controlled by a homemade coverslide containing circulating water attached to the top of the chamber (Fisher Scientific Isotemp 4100). The chamber was connected to a function generator (Agilent 33220A) to produce the desired AC or DC electric field.

2. Drum–like vesicle shapes in DC pulses

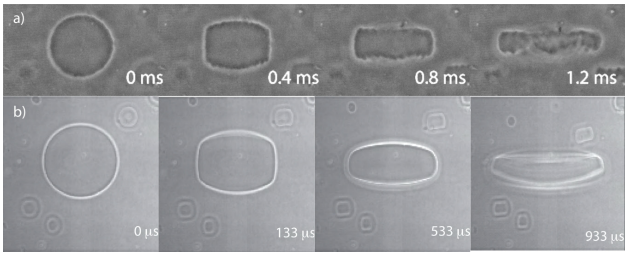

Fig. 2. (a) Lipid vesicle (POPC, radius 15 μm) in a $E_0 = 2kV/cm$ $2ms$ DC pulse. (b) Polymer vesicle (PS1, radius 18 μm) in $E_0 = 4kV/cm$ $5ms$ DC pulse.

Experiments with giant unilamellar vesicles in pulsed DC electric fields revealed peculiar drum-like shapes[7], see Figure 2. We suggest that these shapes reflect a membrane which is porated and conducting in the zone near the poles, and insulating near the equator. The time-evolution of the edge is explained by considering the charging transmembrane voltage. Poration occurs when the transmembrane potential exceeds a critical value, V_c, ranging from about $1V$ for lipid bilayers[8,9] to $9V$ for polymersomes[10]. The position dependent transmembrane potential causes poration where $V_{mm}(\theta) > V_c$, hence there will be a porated region around the pole and a non-porated region around the equator. The membrane properties (tension, bending rigidity, voltage) change drastically from the porated to the intact regions and this discontinuity likely causes the formation of the edge. For example, the electrotension in the membrane is $\sigma_e = C_m V_m^2/2$; its magnitude is significantly lower in the porated (conducting) than in the intact (insulating) regions. The angular position where $V_{mm} = V_c$ corresponds to the edge location θ_c, which from Eq.(3) is found to be

$$\theta_c = \arccos\left(\frac{2V_c}{3(1-\exp(-t/t_{\rm mm}))aE_0}\right). \tag{4}$$

The experimental data in Figure 3 show the edge and the expanse of the conducting zone evolve in time towards the vesicle equator. The porated region also progressively increases with field strength. The data are fit using Eq.(4) with one value for V_c, listed in Table I. Eventually, the conducting area destabilizes the membrane and may lead to collapse and possible vesicle disintegration.

Name	M_n (kDa)	C_m (μF/cm^2)	V_c (V)	$\sigma_{\rm lys}$ (N/m)
PC	0.760	0.710	2.0	0.017
PS1	1.2-b-0.6	0.270	4.2	0.024
PS2	1.8-b-0.9	0.227	6.5	0.048
PS3	2.5-b-1.5	0.172	7.0	0.042
PS4	6.5-b-3.9	0.066	16.0	0.084

Table 1. Membrane capacitance, critical transmembrane voltage, and estimated lysis tension for lipid and polymer systems PBd$_n$-b-PEO$_m$ (PS). The values of the membrane capacitance are taken from[11]. V_c is determined from fitting the time evolution of the edge angle θ_c.

The value of V_c for DOPC used to fit our data (2 V) is about twice the value of found in previous measurements[10,12], and it agrees with recent MD simulations[13,14]. The difference between V_c from our fit and the literature is likely due

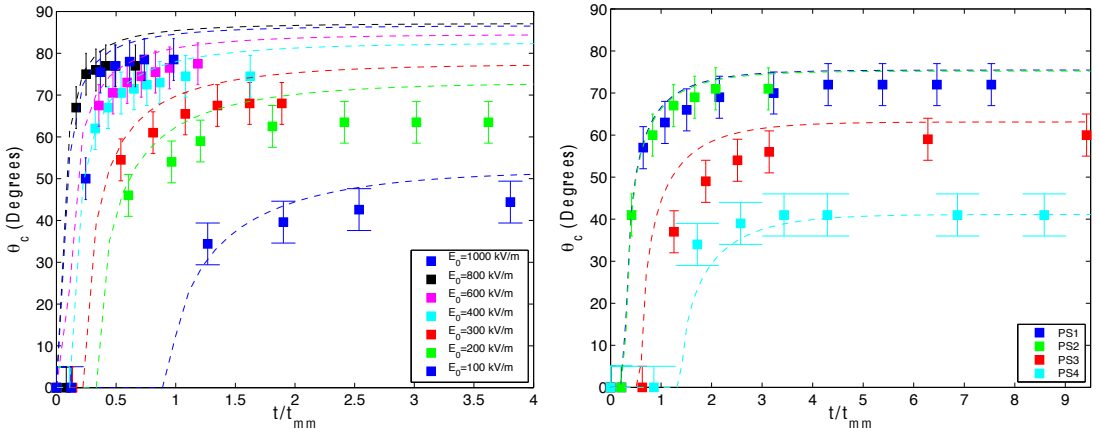

Fig. 3. a) Time-evolution of the edge location θ_c for DOPC vesicles. Lines are data fit with $V_c = 2V$. b)Critical angle time evolution for polymer systems. The electric field strength is $E_0 = 5\,kV/cm$ for PS1 and $E_0 = 6\,kV/cm$ for PS2, PS3, and PS4. The data is fit with one value of V_c for each polymer (see Table 1). The conductivities are $\lambda_{\text{in}} = 4\mu S/cm$, $\lambda_{\text{ex}} = 70\mu S/cm$ for all systems.

to the assumption in the model that the vesicle is a sphere and the field does not change due to the porated regions. For the polymersomes, with the exception of the highest molecular weight polymer, the range of critical membrane potentials is within the range reported in the literature, $V_c \sim 4 - 9V$ [10]. The obtained values also follow the expected trend that the critical transmembrane voltage increases with polymer molecular weight. The knowledge of membrane capacitance [11] and poration voltage allows us to estimate the lysis tension $\sigma_{\text{lys}} = \frac{1}{2}C_m V_c^2$, also listed in Table 1.

3. Shape fluctuations in AC electric field

Lipid membranes are soft and easily bent by thermal noise. Equilibrium shape fluctuations of quasi–spherical vesicles, observed using optical microscopy, are widely used to determine membrane properties, specifically bending rigidity and membrane tension [15,16].

In the presence of electric fields, membrane undulations are modified because of the electric stresses in the membrane. It is predicted that the induced charge on the membrane surface will increase bending rigidity and lower tension [17,18]. The change in the membrane mechanical properties is characterized by adding an electric contribution to the inherent value (in the absence of electric field)

$$\kappa_{eff} = \kappa + \kappa^{\text{el}}, \quad \sigma_{eff} = \sigma - \sigma^{\text{el}}. \tag{5}$$

The effect of electric fields on membrane properties has been studied theoretically [17], but experimental observations are limited. Suspended planar membranes in an electric field were studied using neutron scattering [19]. The results confirmed the increase in bending rigidity and decrease in membrane tension in low conducting solutions. Fluctuations of a quasi–spherical vesicle in an electric field, however, have not been studied. The challenge arises from the fact that the electric field causes the vesicle to deform into an ellipsoid thereby flattening membrane undulations.

We have previously observed that vesicles with $R < 1$ change shape from a prolate to oblate ellipsoid as the frequency of the uniform AC field increases. The transition occurs at a critical frequency f_c, at which the vesicle is a sphere. This frequency is unique because the vesicle has a nonzero transmembrane voltage as well as an effective net charge on the membrane surface. Since there is no net deformation and fluctuations can be observed optically they can be recorded and analyzed using techniques previously developed for the equilibrium fluctuations quasi–spherical vesicles [15,20]. However, since the presence of the electric field essentially drives the system out of equilibrium [21], we also measure the temporal correlations of membrane fluctuations. This provides an alternative method to determine bending rigidity and tension [22].

3.1. Analysis of the shape fluctuations of a quasi–spherical vesicle

The membrane position for each frame is given in polar coordinates $r(\theta, t)$, where the centroid is determined from the contour data [15]. The radial contour information is converted into a height function, $h(\theta, t)$, defined as the deviation from a mean position. The mean radius for each frame is averaged over the entire contour,

$$h(\theta, t) = r(\theta, t) - \langle r(t) \rangle_\theta \,, \tag{6}$$

where $\langle\rangle_\theta$ denotes average over θ. The height-height temporal correlation function is found by [15],

$$C(n, \Delta t) = \langle |h(n, t)||h(n, t + \Delta t)| \rangle_t - \langle |h(n, t)| \rangle_t^2 \,, \tag{7}$$

where $\langle\rangle_t$ denote average over time and n is the mode number ($n = aq$). The temporal correlation function is normalized by $C(n, \Delta t = 0)$ to isolate the effect of the relaxation rates,

$$C_{\text{norm}}(n, \Delta t) = \frac{C(n, \Delta t)}{C(n, \Delta t = 0)}. \tag{8}$$

The normalized function is then compared the dynamical correlation function derived for a spherical geometry [23,24],

$$C_{\text{norm}}(n, \Delta t) = \exp\left(-\zeta_1(n)\Delta t\right) \,, \tag{9}$$

where

$$\zeta_1(n) = \left[\frac{n(n+1)}{\mu a^3 (2n+1)(2n^2+2n-1)}\right](n+2)(n-1)[\kappa(n+1)n + \sigma a^2] \,. \tag{10}$$

The relaxation rates are determined as a function of mode number. Then this data is fit to the theoretical expression for $\zeta_1(n)$, to get bending rigidity and tension using a least squares method.

The objective is to observe how the electric field modifies $\zeta_1(q)$ and determine renormalized values for κ and σ. Note that the current measurements are spatially averaged over the entire vesicle and that a spatial dependence in the effective membrane properties may exist because of the angular dependence on the transmembrane potential with respect to the applied field.

3.2. Experimental procedure

DOPC vesicles are observed using a phase contrast microscope Axio Observer.A1 with 100x 1.2 NA oil immersion objective. The high speed camera records membrane fluctuations at 125 frames per second (fps) and has a shutter speed of 1/5000 seconds [16]. The use of the faster shutter reduces the influence of integration time errors which can create a blurred image during recording [15]. 6000-8000 frames are recorded for each experiment, approximately one minute of recording time. The membrane contour is found using a sub-pixel resolution contour recognition software [16].

The range of mode numbers used for most vesicles is within $n \sim 6 - 18$. The lowest modes can be influenced by the coverslip while the highest modes are limited by resolution. A set of images recording membrane fluctuations is first taken in the absence of electric fields. An AC field is then applied at the transition frequency, which is determined by adjusting the frequency until the vesicle remains spherical. The field strength is increased in increments of 1 kV/m from $E_0 = 1 - 5$kV/m. A final measurement is taken after the field is turned off to confirm that the membrane properties have not changed due to the application of the electric field. A full set of 6000-8000 frames are recorded at each field strength.

Measurements at field strengths higher than 5 kV/cm are difficult due to interactions between vesicles. The vesicles begin to attract each other in strong fields resulting from interactions between the induced dipoles on the vesicles. The vesicles will align in pearl chain formations and disrupt membrane fluctuations. Measurements where vesicles come in contact with surrounding vesicles are discarded.

3.3. Results

The procedure outlined in the previous section is used to measure the bending rigidity and tension for DOPC vesicles with and without electric fields. The correlation function determined from experiments using Eq.(8) is compared

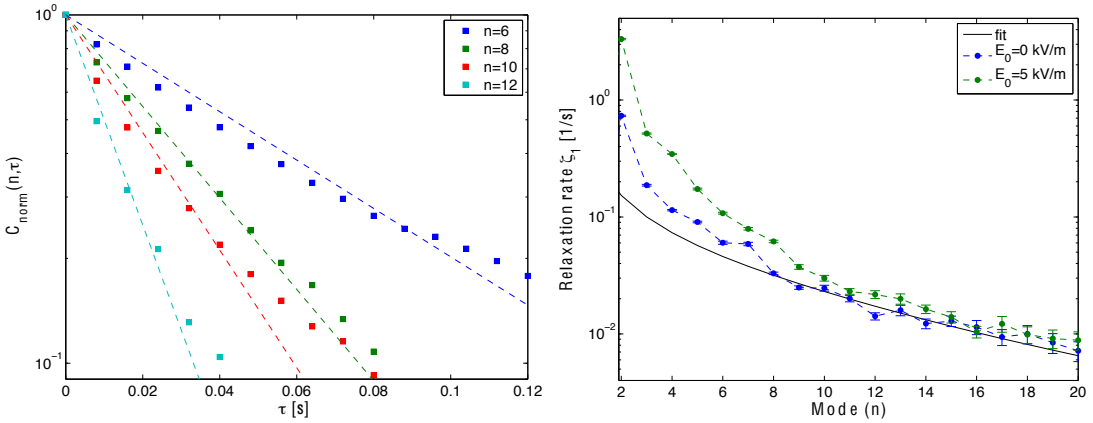

Fig. 4. a) Normalized correlation function for a DOPC vesicle. Average radius of the vesicle is a=14.3 μm. The symbols represent experimental data calculated using Eq.(8) and the lines are the fits of the data for each mode number using Eq.(9); the slopes yield $\zeta_1(n)$. b)Relaxation rates as a function of modes n. Theoretical curve if the fit with Eq.(10). The relaxation rates for a a =14.3 μm DOPC vesicle with and without electric field are compared.

to the exponential decay predicted by Eq.(9). The results show fairly good agreement with the exponential decay predicted by Eq.(9). The recording rate limits the number of points that can be used to fit the higher mode numbers. An acquisition rate greater than 125 fps could be used, but this would reduce the total amount of observation time due to the limit on frames that can be recorded.

Each mode is described by Eq.(9) using the relaxation rate ζ_1 as a fitting parameter, see Figure 4.a). Figure 4.b) shows the obtained relaxation rate as a function of mode number. The errors associated with the exponential fits are determined from a 90% confidence interval. The higher modes have a larger error due to the fewer number of points available to fit. The lack of agreement for the lowest modes is likely due to the influence of the chamber wall (vesicles have slightly higher density than the suspending solution and therefore sediment to the bottom). The highest modes appear to follow the fitted expression, but the error begins to become large due to the lack of temporal and spatial resolution.

Figure 5 shows the bending rigidity and tension determined from these fits for a set of experiments on one vesicle at different field strengths. The bending rigidity without electric field is found to be within the range of previous measurements for DOPC, $\kappa \approx 20 - 25\, k_B T$ [16]. All measurements before and after application of the electric field were consistent within the margin of error of the fluctuation analysis. The bending rigidity is observed to increase with field strength while the effective tension decreases with electric field strength. The bending rigidity value at the highest electric field strength (5 kV/m) is roughly twice the original bending rigidity. The highest field strength decreases the tension to less than half the original value.

The effect of the electric field on membrane properties is likely to scale with electric stress, which depends quadratically on the electric field strength. The curves plotted in Figure 5 are effective membrane property values assuming the form given in Eq.(5) and that $\kappa^{\mathrm{el}} \sim E_0^2$ and $\sigma^{\mathrm{el}} \sim E_0^2$. The coefficients given in Figure 5 are estimates based on the magnitude of change seen in the results. Although the change in membrane properties do not agree closely with the E_0^2 scaling, the general trends of increasing bending rigidity and decreasing tension are observable.

4. Electrotension regulated phase behavior in biomimetic tri-component membranes

Artificial lipid bilayers made of mixtures of lipids and cholesterol are widely studied as a model of raft formation in cellular membranes [25]. Membranes consisting of a high-melting temperature lipid, a low melting temperature lipid, and cholesterol can phase separate to form domains. This process has been extensively studied as a function of temperature and composition [26]. Only recently have the effect of tension on membrane phase behavior has been measured, but the experimental results are conflicting [27,28]. Here we study the effect of electric-field induced tension in the membrane on the melting transition.

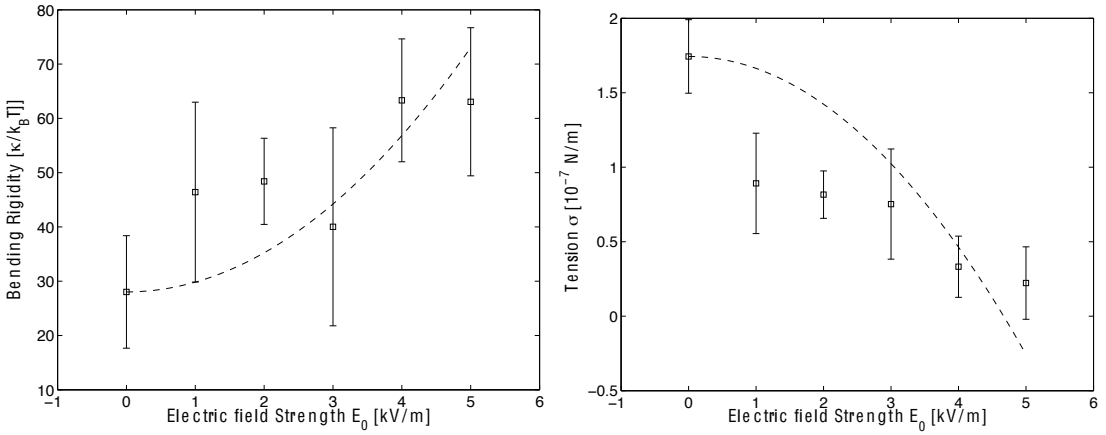

Fig. 5. Bending rigidity (left) and membrane tension (right) as a function of field strength for one vesicle. The effective bending rigidity given by Eq.(5) is plotted for $\kappa^{\rm el} = 1.8[k_BT/(kV/m)^2]E_0^2$. The effective tension is plotted for $\sigma^{\rm el} = 0.08 \times 10^{-7}[N/m/(kV/m)^2]E_0^2$. E_0 is the electric field in kV/m.

The lipid solution was composed of a ternary mixture of DOPC, DPPC, and Cholesterol in a 2:2:1 molar ratio with 0.1 mol % of the fluorescent lipid Rh-DOPE . Rh-DOPE preferentially partitions into the DOPC enriched L_d phase, thereby exposing the L_o domains as dark spots within the bright membrane as the temperature is lowered through the miscibility transition $T_m \sim 34°\mathrm{C}$[29,26]. Above T_m, the membrane is in one homogenous liquid phase.

To minimize photo-induced effects, such as peroxidation of unsaturated lipids[30], we used phase contrast whenever possible throughout the experiment and the fluorescent lamp was shuttered as to only expose vesicles at the moment of image acquisition. Taking these precautions allowed imaging of the vesicles every 4 seconds for up to 30-40 minutes without signs of artificial domain formation.

Experiments were started by lowering the chamber temperature through the miscibility transition of a vesicle. The chamber was then set to a constant temperature T_2 below T_m. A low frequency (100 Hz) AC electric field was applied, increasing in magnitude until domains dissolved and the vesicle returned to a homogenous phase. The magnitude of the field was then lowered every 40 s until a critical field strength (E_{cr}) at which the domains reformed. Figure 6 shows a typical observation. This process was repeated on multiple vesicles for different values of T_2. The range of T_2 was limited by the function generator's maximum voltage and the physical strength of the membranes (poration voltage $V_c \sim 1.1\ V$).

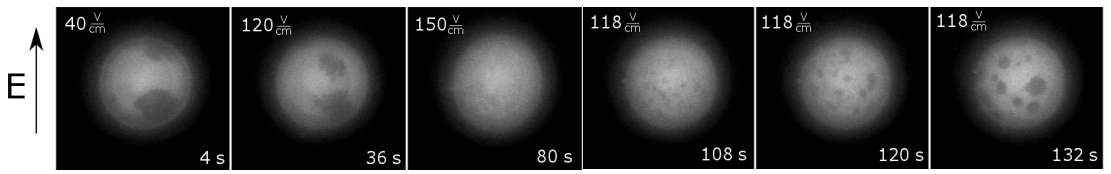

Fig. 6. Fluorescent images from single experiment at constant temperature $T = 31.4°\mathrm{C}$. The strength of the electric field is in the top left corner of each image.

The results are shown in Figure 7, displayed as the change in miscibility temperature, $\Delta T = T_2 - T_m$, versus the critical field strength of domain reformation, E_{cr}. Each point represents one test on an individual vesicle. Increasing the magnitude of ΔT very clearly led to a higher critical field strength at which the domains reformed. The variance in E_{cr} can be explained by the different values of initial tension of each vesicle.

The decrease in T_m with electric field strength can be explained by considering the electric–field induced tension in the membrane[31]

$$\sigma_e = \epsilon_m\epsilon_0\left(\frac{h}{2h_e^2}\right)V_m^2 \sim (a^2/h)E_0^2, \tag{11}$$

where ϵ_m is the relative permittivity of the membrane, ϵ_0 is the vacuum permittivity, h is the thickness of the bilayer, and h_e is the thickness of the hydrophobic core. Uline *et al.* (2012)[32] calculated the change in miscibility temperature with membrane tension for a DOPC/DPPC/Chol system as $(dT/d\sigma) = -1.0\ K(pN/nm)^{-1}$.

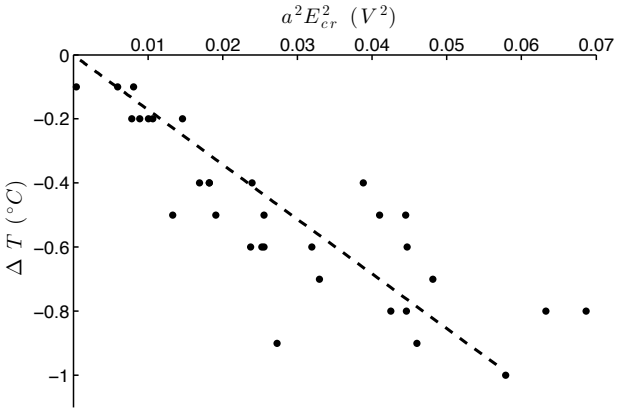

Fig. 7. Change in miscibility temperature plotted as a function of $a^2E_0^2$. The dashed line represents the theoretical change in miscibility temperature calculated using Eq.(12) with the values $h = 67$ Å, $h_e = 28$ Å, $\epsilon_m = 2$, $\epsilon_0 = 8.85 \cdot 10^{-12}\ F/m$[33].

Combining this result with Eq.(11) yields a theoretical prediction for the change in miscibility temperature with applied electric field, E_0

$$\Delta T = -(10^3)\left(\frac{9}{8}\right)\epsilon_m\epsilon_0\left(\frac{h}{h_e^2}\right)a^2E_0^2 = (-17.02)\ a^2E_0^2 \tag{12}$$

where we have used $h = 67$ Å, $h_e = 28$ Å, $\epsilon_m = 2$, $\epsilon_0 = 8.85 \cdot 10^{-12}\ F/m$[33].

Figure 7 compares the experimental data with Eq.(12). The agreement is excellent, which is very encouraging considering that there are no fitting parameters.

5. Instability in low frequency AC electric field

Experiments investigating the behavior of vesicles in elongational flow have shown a stretching transition to a dumbbell shape for very deflated vesicles[34]. Low frequency electric fields, and intermediated frequencies for vesicles with $R > 1$, produce electric stresses similar to elongation flow. Preliminary experiments on very deflated POPC vesicles in 100 Hz AC fields demonstrates a similar transition, see Figure 8.

After the field is turned on, the vesicle separates into two daughter vesicles connected by a lipid tether. The instability was observed to be asymmetric, with one daughter vesicle noticeably larger than the other. After the instability, the two vesicles begin to equalize and the tether becomes smaller as area is pulled into the vesicle. It was observed that in some vesicles, the two daughter vesicles rejoined and the instability repeats. Other vesicles stay separate as two equal sized daughter vesicles. The symmetry breaking leading to the formation of a vesicle dumbbell is somewhat reminiscent of the behavior of interconnected rubber balloons[36]: two identical balloons allowed to exchange air (though a connecting pipe) can evolve into a stable equilibrium where the two balloons have different size, an effect due to the non-monotonic dependence of the membrane tension on inflation. A more detailed study for different values of vesicle excess area and applied electric field strength is needed in order to understand the mechanism of this instability.

6. Conclusions

We have experimentally studied the electric–field induced deformation of fluid bilayers, mimicking the biological membranes. DC pulses are found to drive formation of edges, which our results suggest separate porating and intact

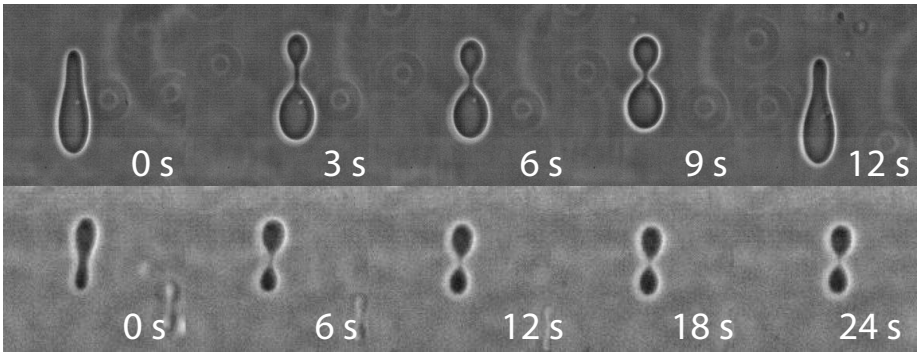

Fig. 8. Time snapshots of the transition to an asymmetric (top) or symmetric (bottom) dumbbell shape for a deflated vesicle in a 100 Hz 20 kV/m electric field. Very small translational oscillations in the experiments occurred at low frequencies (f $\lessapprox$ 100 Hz), likely caused by small but non-negligible surface charge of the PC lipids [35].

regions of the membranes. Shape fluctuations in AC fields provide means of estimating the renormalization of the membrane mechanical properties (bending rigidity and tension) due to the transmembrane electric field: we find an increase in effective bending rigidity and a decrease in effective tension. The electric-field induced tension affects phase transitions in fluid membranes, namely, it lowers the miscibility temperature. Finally, we observe that a deflated vesicle can adopt asymmetric dumbbell shape in the uniform AC electric field, a phenomenon that awaits explanation.

Acknowledgements

This work has been financially supported by NSF-CBET 1117099 and NSF- CMMI 1232477.

References

1. Grosse, C., Schwan, H.P.. Cellular membrane potentials induced by alternating fields. *Biophys J* 1992;**63**:1632–1642.
2. Schwan, H.P.. Dielectrophoresis and rotation of cells. In: Neumann, E., Sowers, A.E., Jordan, C.A., editors. *Electroporation and electrofusion in cell biology*. Plenum Press; 1989, p. 3–21.
3. Kinosita Jr., K., Ashikawa, I., Saita, N., Yoshimura, H., Itoh, H., Nagayama, K., et al. Electroporation of cell membrane visualized under a pulsed laser fluorescence microscope. *Biophys J* 1988;**53**:1015–1019.
4. Schwalbe, J.T., Vlahovska, P.M., Miksis, M.J.. Vesicle electrohydrodynamics. *Phys Rev E* 2011;**83**(4):046309.
5. McConnell, L.C., Miksis, M.J., Vlahovska, P.M.. Vesicle electrohydrodynamics in dc electric fields. *IMA J Appl Math* 2013;**78**(4):797–817.
6. Seiwert, J., Miksis, M.J., Vlahovska, P.M.. Stability of biomimetic membranes in dc electric fields. *J Fluid Mech* 2012;**706**:58–70.
7. Riske, K.A., Dimova, R.. Electric pulses induce cylindrical deformations on giant vesicles in salt solutions. *Biophys J* 2006;**91**:1778–1786.
8. Needham, D., Hochmuth, R.M.. Electromechanical permeabilization of lipid vesicles. role of membrane tension and compressibility. *Biophys J* 1989;**55**:1001–1009.
9. Dimova, R.. *Membrane Electroporation in High Electric Fields*; chap. 7. Wiley-VCH Verlag GmbH & Co. KGaA. ISBN 9783527644117; 2011, p. 335–367.
10. Aranda-Espinoza, H., Bermudez, H., Bates, F.S., Discher, D.E.. Electromechanical limits of polymersomes. *Phys Rev Lett* 2001;**87**:208301.
11. Salipante, P.F., Knorr, R.L., Dimova, R., Vlahovska, P.M.. Electrodeformation method for measuring the capacitance of bilayer membranes. *Soft Matter* 2012;**8**(14):3810–3816.
12. Riske, K.A., Dimova, R.. Electro-deformation and poration of giant vesicles viewed with high temporal resolution. *Biophys J* 2005; **88**:1143–1155.
13. Ziegler, M.J., Vernier, P.T.. Interface water dynamics and porting electric fields for phospholipid bilayers. *J Phys Chem B* 2008; **112**(43):13588–13596.
14. Fernández, M.L., Marshall, G., Sagués, F., Reigada, R.. Structural and kinetic molecular dynamics study of electroporation in cholesterol-containing bilayers. *J Phys Chem B* 2010;**114**(20):6855–6865.
15. Pecreaux, J., Dobereiner, H.G., Prost, J., Joanny, J.F., Bassereau, P.. Refined contour analysis of giant unilamellar vesicles. *Eur Phys J E* 2004;**13**:277–290.
16. Gracia, R.S., Bezlyepkina, N., Knorr, R.L., Lipowsky, R.L., Dimova, R.. Effect of cholesterol on the rigidity of saturated and unsaturated membranes: fluctuation and electrodeformation analysis of giant vesicles. *Soft Matter* 2010;**6**:1472 – 1482.
17. Ziebert, F., Lacoste, D.. A planar lipid bilayer in an electric field: Membrane instability, flow field, and electrical impedance. In: Iglic, A., editor. *Advances in Planar Lipid Bilayers and Liposomes*; vol. 14. Elsevier; 2011, p. 63–95.

18. Ambjornsson, T., Lomholt, M.A., Hansen, P.L.. Applying a potential across a biomembrane: Electrostatic contribution to the bending rigidity and membrane instability. *Phys Rev E* 2007;**75**:051916.
19. Lecuyer, S., Fragneto, G., Charitat, T.. Effect of an electric field on a floating lipid bilayer: A neutron reflectivity study. *Eur Phys J E Soft Matter* 2006;**21**(2):153–159.
20. Méléard, P., Pott, T., Bouvrais, H., Ipsen, J.H.. Advantages of statistical analysis of giant vesicle flickering for bending elasticity measurements. *Eur Phys J E Soft Matter* 2011;**34**(10):1–14.
21. Vlahovska, P.M.. Non-equilibrium dynamics of lipid membranes: deformation and stability in electric fields. In: Iglic, A., editor. *Advances in Planar Lipid Bilayers and Liposomes, vol. 12*. Elsevier; 2010, p. 103–146.
22. Zhou, H., Gabilondo, B.B., Losert, W., van de Water, W.. Stretching and relaxation of vesicles. *Phys Rev E* 2011;**83**(1):011905.
23. Schneider, M.B., Jenkins, J.T., Webb, W.W.. Thermal fluctuations of large quasi-spherical bimolecular phospholipid vesicles. *J Phys (France)* 1984;**45**(9):1457–1472.
24. Milner, , Safran, . Dynamical fluctuations of droplet microemulsions and vesicles. *Phys Rev A* 1987;**36**:4371–4379.
25. Dietrich, C., Bagatolli, L.a., Volovyk, Z.N., Thompson, N.L., Levi, M., Jacobson, K., et al. Lipid rafts reconstituted in model membranes. *Biophys J* 2001;**80**:1417–28.
26. Veatch, S.L., Keller, S.L.. Separation of liquid phases in giant vesicles of ternary mixtures of phospholipids and cholesterol. *Biophys J* 2003;**85**:3074–83.
27. Hamada, T., Kishimoto, Y., Nagasaki, T., Takagi, M.. Lateral phase separation in tense membranes. *Soft Matter* 2011;**7**:9061–9068.
28. Portet, T., Gordon, S.E., Keller, S.L.. Increasing membrane tension decreases miscibility temperatures; an experimental demonstration via micropipette aspiration. *Biophys J* 2012;**103**:L35 – L37.
29. Baumgart, T., Hunt, G., Farkas, E.R., Webb, W.W., Feigenson, G.W.. Fluorescence probe partitioning between Lo/Ld phases in lipid membranes. *Biochim Biophys Acta* 2007;**1768**:2182–94.
30. Ayuyan, A.G., Cohen, F.S.. Lipid peroxides promote large rafts: effects of excitation of probes in fluorescence microscopy and electrochemical reactions during vesicle formation. *Biophys J* 2006;**91**:2172–83.
31. Dimova, R., Riske, K.A., Aranda, S., Bezlyepkina, N., Knorr, R.L., Lipowsky, R.. Giant vesicles in electric fields. *Soft matter* 2007; **3**:817–827.
32. Uline, M.J., Schick, M., Szleifer, I.. Phase behavior of lipid bilayers under tension. *Biophys J* 2012;**102**:517–22.
33. Nagle, J.F., Tristram-Nagle, S.. Structure of lipid bilayers. *Biochim Biophys Acta* 2000;**1469**:159–195.
34. Kantsler, V., Segre, E., Steinberg, V.. Critical dynamics of vesicle stretching transition in elongational flow. *Phys Rev Lett* 2008; **101**(4):48101.
35. Pincet, F., Cribier, S., Perez, E.. Bilayers of neutral lipids bear a small but significant charge. *The European Physical Journal B-Condensed Matter and Complex Systems* 1999;**11**(1):127–130.
36. Mueller, I., Strehlow, P.. Rubber and rubber balloons. *Lect Notes Phys* 2004;**637**:1–5.